ELSEVIER

Surface Science 388 (1997) 110–120

surface science

The role of stress in the heteroepitaxy of Au on W(110)

M.L. Hildner *, K.E. Johnson, R.J. Wilson

IBM Research Division, Almaden Research Center, 650 Harry Road, San Jose, CA 95120-6099, USA

Received 20 December 1996; accepted for publication 28 April 1997

Abstract

The role of stress in forming a variety of Au film structures on W(110) is examined with scanning tunneling microscopy (STM). The structural manifestations are different from those previously observed with STM because this system involves both an fcc(111)/bcc(110) interface that has mixed (tensile and compressive) strain and the Au(111) surface which reconstructs through strain relaxation. Whereas sub-monolayer films already show isotropic strain relaxation through a combination of three uniaxial expanded structures, the complete monolayer is pseudomorphic. Strain relaxation then leads to a two-dimensional dislocation structure in the bilayer film and a non-bulk-like yet fully strain-relaxed trilayer film. Stress is reintroduced for subsequently thicker films; this leads to the growth of flat-topped three-dimensional crystallites, none of which are terminated by the fourth layer, and to the eventual formation of the uniaxially compressed surface reconstruction of Au(111). © 1997 Elsevier Science B.V.

Keywords: Epitaxy; Gold; Low index single crystal surfaces; Metallic films; Scanning tunneling microscopy; Surface relaxation and reconstruction; Surface stress; Tungsten

1. Introduction

The structures of surfaces and of epitaxially grown films are often dictated by the presence of stress. For single-crystal surfaces, stress is caused by the loss in coordination of atoms at the solid–vacuum interface and, if energetically favorable, can be relieved by atomic rearrangement [1]. In heteroepitaxy, the stress arises from the lattice mismatch between the substrate and film. Here, the film structure is determined by a subtle balance between E_ϵ, the energy of the elastic strain associated with a pseudomorphic film, and E_r, the interface energy associated with a relaxed, non-pseudomorphic interface [2,3]. In metal-on-metal systems with small lattice mismatch, E_ϵ of initial layers is often sufficiently smaller than E_r for the film to be pseudomorphic or commensurate. As the film thickens, E_ϵ increases and, after reaching a critical film thickness, the stress can be relieved by the formation of a weakly incommensurate phase consisting of misfit dislocations separating larger areas which are nearly commensurate. If E_ϵ becomes much larger than E_r, an incommensurate relaxed film can result.

For surfaces, the quintessential example of a stress relieved reconstruction occurs on the (111) surface of gold [1,4]. The reconstructed $(22 \times \sqrt{3})$ unit cell consists of two dense domain walls that separate larger areas that alternate between fcc and hcp stacking. The 4% compression is, on a local scale, unidirectional (along $[0\bar{1}1]$) and with

* Corresponding author. Present address: University of Maryland, Laboratory for Physical Sciences, College Park, MD 20742-4111, USA. Fax: (+1) 301 935.6723; e-mail: hildner@surface.umd.edu

PII S0039-6028(97)00382-8

fcc sites more energetically favorable than hcp sites, a paired stripe arrangement along [$\bar{2}11$] arises. The relaxation is made more isotropic over long length scales – the domain walls bend by $\pm 120°$ and form the so-called herringbone structure [5]. For epitaxial films, recent scanning tunneling microscopy (STM) studies have revealed a sequence of film structures resulting from the relaxation of tensile strain at metal-on-metal hexagonal interfaces. Cu films on Ru(0001) were observed to evolve from an initial pseudomorphically strained single-layer film to a fully relaxed bulk-like Cu four-layer film through a series of films in which the strain is relieved either unidirectionally or more isotropically through the formation of high density misfit dislocations [3]. Similar structural manifestations for films relaxing from compressive stress have also been observed with STM but with low density misfit dislocations [3,6].

Stress also plays a role in determining the thermodynamic epitaxial growth mode. In the thermodynamic limit, the mode is determined by the interrelationship of the surface free energies of the substrate and n-layer film, γ_s and $\gamma_{f,n}$ respectively, and the interfacial energy, $\gamma_{i,n}$, which contains the thickness dependent strain energy of the film. Layer-by-layer or Frank–Van der Merwe (FM) growth is expected if $\gamma_s \geq \gamma_{f,n} + \gamma_{i,n}$. In heteroepitaxial systems, the strain energy increases with n so that the FM condition will no longer be valid at a critical film thickness n^* and three-dimensional (3D) crystals form (Stranski–Krastanov (SK) mode). The Volmer–Weber (VM) mode, where 3D growth begins immediately, corresponds to $n^* = 1$.

In this paper, we describe the structural manifestations observed by STM in epitaxial Au/W(110) that arise from the relaxation of the mixed (tensile and compressive) strain at this fcc(111)/bcc(110) interface. A fully strained pseudomorphic Au lattice – with Au[$0\bar{1}1$]‖W[$00\bar{1}$] – would have a negative misfit of -8.7% along W[001] and a positive misfit of 11.8% along the perpendicular W[$\bar{1}10$] direction in addition to the positive misfit of 5.4% along both W[$1\bar{1}1$] and W[$\bar{1}11$]. Therefore, in reference to the W lattice, compression along [001] and expansions along [$\bar{1}10$], [$1\bar{1}1$] and [$\bar{1}11$] are expected, and indeed observed, as the Au film relaxes with increasing thickness. This mixture of expansion and compression leads to previously unobserved weakly incommensurate phases in the first two layers. Three-layer films are essentially fully relaxed yet non-bulk-like, but the accompanying transition of the underlying second layer occurs as a function of layer three coverage. The SK growth mode is observed with a critical thickness of four, yet the flat topped crystallites that form never show a fourth layer top. As strain relaxation proceeds in thicker crystallites, surface dislocations emerge and evolve into the uniaxial compression structures of the Au(111) surface.

2. Experimental

The STM and ultrahigh-vacuum system have been described elsewhere [7]. Au films were evaporated from an alumina-coated W basket at a rate of ~ 0.1 Å s^{-1}. This rate was monitored with an ion gage and calibrated with the STM. Films deposited at room temperature (RT) were rough, showing kinetically limited multilayer growth. On the other hand, as the STM images will show, films that were subsequently annealed to 500°C showed characteristics of thermodynamic growth. This indicates that the structures observed under these conditions are energetically favored and driven by strain relaxation. All images shown were obtained at RT following an anneal to 500°C. The constant current mode was used with 0.1–1.5 V positive or negative tip bias and tunnel currents of 0.5–2.0 nA.

3. Results and discussion

For Au films of less than one monolayer (ML), the surface is marked by numerous holes scattered about on partially filled terraces, as shown in Fig. 1a. There is also a subtle texturing in the form of bright ridges perpendicular to [$1\bar{1}1$] and [$\bar{1}11$] and shallow troughs along [001]. These features are only 0.2 Å high, occur at distances around 20 Å, and are frequently interrupted by the interspersed holes. As the coverage is increased to 1.5 ML, the holes fill in to result in smooth regions

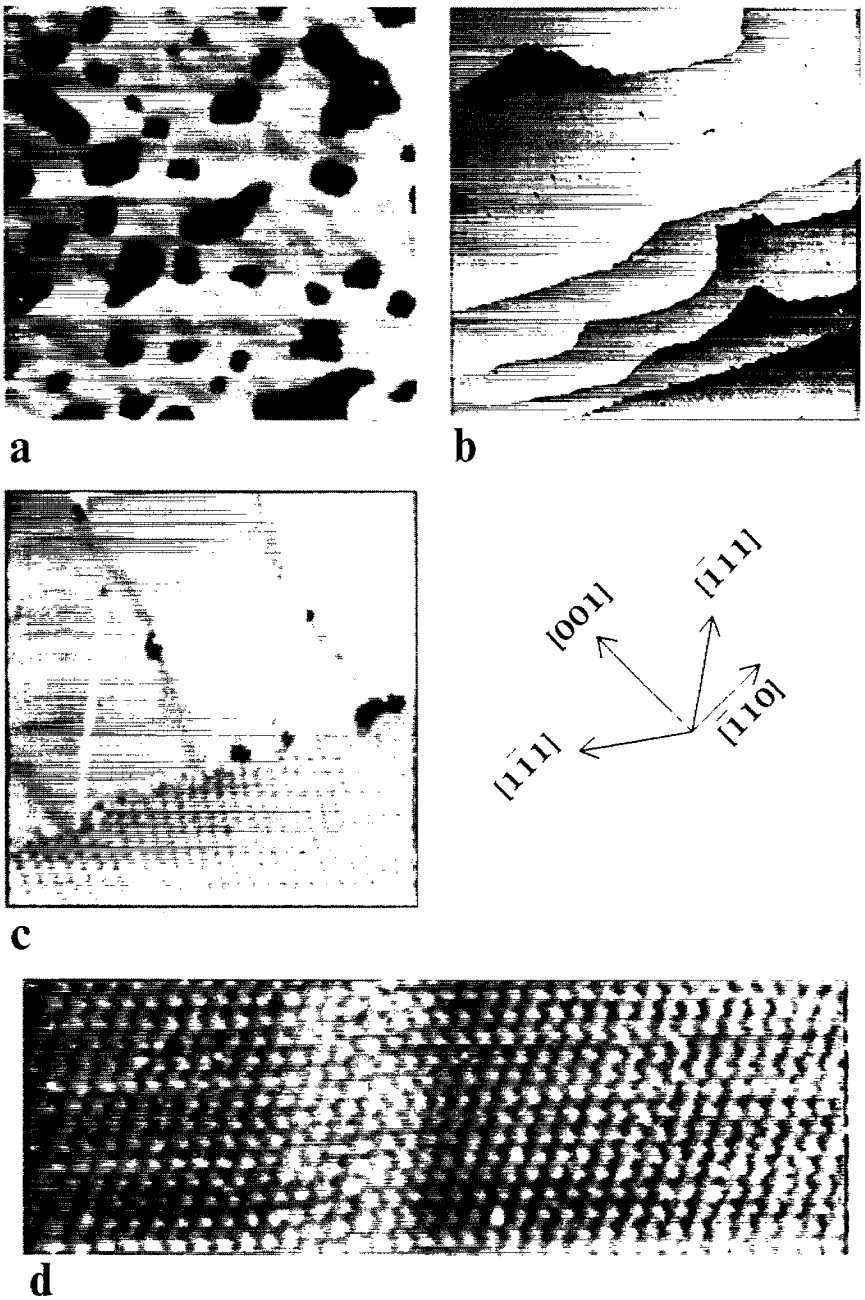

Fig. 1. STM images of layers 1 and 2. The vector diagram shows the orientation of the W(110) crystal for these and all subsequent STM images. (a) (600 Å × 600 Å) image at 0.6 ML shows bright ridges perpendicular to [1$\bar{1}$1] and [$\bar{1}$11] and dark troughs perpendicular to [$\bar{1}$10]. (b) (2000 Å × 2000 Å) and (c) (600 Å × 600 Å) show, at 1.6 ML, a smooth layer 1 that is broken by the same but farther spaced ridges and troughs, and a highly corrugated layer 2 that exhibits step flow growth. (d) (95 Å × 36 Å) atomic-resolution image at 1.6 ML containing a ridge – as the atomic rows traverse the ridge from left to right, they shift upwards by less than the inter-row spacing.

of layer one (L1) growth which are broken up by the same ridges and troughs as at lower coverage, but now spaced by hundreds of ångströms (Fig. 1b and c). The patches between these stripe structures at both coverages show only atomic corrugation with spacings close to or identical to those of the substrate (Fig. 1d), implying that the Au is locally conformal to the W(110) surface. Fig. 1d, an atomic-resolution image of L1 in the vicinity of a ridge, also shows that as the atomic rows cross the bright ridge they shift by less than the inter-row spacing. This implies that the registry of the Au lattice changes across the ridges. To explain this change in registry, we suggest that the Au atoms shift from the hourglass binding site of bcc materials towards the threefold hollow sites preferred by fcc materials of which there are two in the vicinity of each bcc site (these two sites are hereafter called left-handed (LH) and right-handed (RH) threefold sites). The stripes are then readily attributed to misfit dislocations (domain walls) that separate the two types of domain expected.

With this interpretation it is apparent that strain relief appears in the first atomic layer of Au on W(110) and that it decreases with coverage. Fig. 2 shows a schematic of the L1 misfit dislocation structure. The bright ridges are low density walls that create, on a local scale, a uniaxial expansion. The alignment of this expansion alternates between the $[1\bar{1}1]$ and $[\bar{1}11]$ directions. This alternation is reminiscent of the Au(111) herringbone structure, and in similar fashion facilitates a more isotropic strain reduction. However, unlike Au(111), there is no pairing of lines, since the LH and RH threefold sites are energetically equivalent. The increased height for the Au atoms in these walls is explained by their shift away from the LH and RH sites towards bridge sites. The dark troughs are also low density walls and create a uniaxial expansion in the $[\bar{1}10]$ direction. The fact that these walls are imaged as depressions is expected from the increased Au atom spacing and the lack of Au atoms at or near bridge sites.

For drawing simplicity, the domain walls in the model of Fig. 2 are narrower than those seen in the STM images (see Fig. 1d). If the width of the ridges is increased beyond the six atoms of the model, the bond geometry within these walls

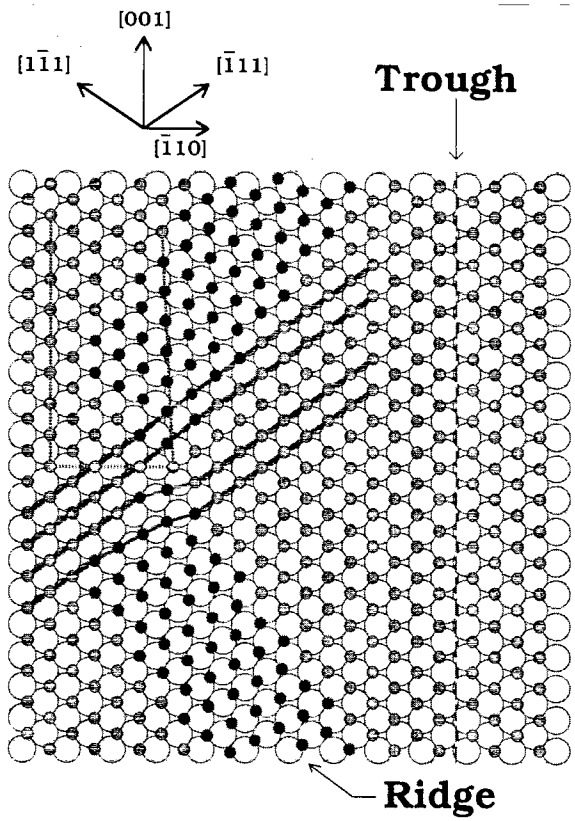

Fig. 2. Model of first layer. Ridges and troughs are domain walls that separate two types of threefold hollow site (RH and LH). To simplify the illustration, both types of domain wall are depicted as narrower than observed in the STM images. The ridges are comprised of uniaxial expansions that alternate between alignments along $[1\bar{1}1]$ (top ridge) and $[\bar{1}11]$ (bottom ridge). The troughs are uniaxial expansions along $[\bar{1}10]$. The dotted lines show that the ridge also provides some compression along [001] – the distance spanned by the same number of atoms is less across than outside a ridge. The gray lines illustrate the 2D edge dislocation formed at the junction of two ridges.

changes. The preferred geometry of fcc Au(111) – hexagonal with 60° bond angles – is obtained at a ridge width of nine atoms. This appears to be the width observed in Fig. 1d.

While not explicit, this structure does have some compression along [001] which is imposed by the ridges. As demonstrated in Fig. 2, an examination along [001] reveals that the distance spanned by a given number of atoms across the ridges is shorter than the distance for the same number of atoms outside the ridges (it is also observed that the

ridges provide expansion along [$\bar{1}$10]). Regardless, there is clearly a stronger tendency toward relaxation of the compressive strain – including that resulting from the comparatively small misfit along the [1$\bar{1}$1] and [$\bar{1}$11] directions – as opposed to the tensile strain in this first layer. This is in accord with previous evidence from studies of isotropically strained interfaces that systems of positive misfit display dislocation structures in earlier layers than those of comparable negative misfit [8]. This phenomenon has been ascribed to the effectiveness of the steeply increasing repulsive Morse potential in preventing film compression [3]. Apparently, this effectiveness is marginal for Au on W(110) since the film becomes (nearly) pseudomorphic at 1 ML.

An additional feature in the sub-monolayer films is the presence of voids at the junctions of the ridges. These are not depicted in the model, but are probably a consequence of a two-dimensional (2D) edge dislocation in the Au lattice formed at these unions. This dislocation creates an extra atomic row (seen along either [$\bar{1}$11] or [1$\bar{1}$1]) inside the triangular-shaped LH domain. In order to accommodate the extra row, the bond geometry inside the junction region must deviate more strongly than elsewhere in the film from the preferred hexagonal one; this makes such sites energetically unfavorable.

The observed structure conflicts with previous structural models [9,10] which were deduced from LEED patterns that we have verified in our measurements. These models predict a uniformly spaced atomic array with lattice spacings that match the W periodicity along W[001] and are slightly longer along W[$\bar{1}$10]; these would clearly give only one-dimensional variations in the overlayer atomic positions. The LEED pattern, which shows superlattice beams spaced along [$\bar{1}$10] and not along [001], arises instead from the superlattice of triangular domains being well correlated along [$\bar{1}$10] but irregularly spaced along [001], as can be seen in Fig. 1a.

The bilayer film can be seen in Fig. 1b and c. As seen in Fig. 1b, this film has a second layer that is more highly corrugated, commences at the initial positions of the underlying substrate steps – which are clearly marked by rows of pinholes – and extends to smooth growth fronts of the step flow type. Fig. 1b also suggests that the underlying first layer of the film remains pseudomorphic, as there are no distortions in L1 in front of the layer two (L2) growth fronts. The atomic resolution image of Fig. 3a shows that L2 forms large perfect single domains which extend for hundreds of ångströms. The continuous bright ridges in these domains exhibit a "square wave" pattern that runs roughly along the [001] direction. There are also vacancy rows, in periodic arrangement, that occur wherever neighboring square waves approach contact.

The precision of the periodic structures implies that L2 forms a weakly incommensurate phase that is locked into registry with the substrate on a length scale of tens of atoms. The ridges in the square wave pattern can then be ascribed to misfit dislocation structures separating regions where the second layer Au is nearly conformal to the underlying pseudomorphic first layer. It is tempting to model the transverse and longitudinal ridge segments as uniaxial compressions and uniaxial expansions respectively, as this would provide for a packing that is closer along [001] and expanded in the perpendicular [$\bar{1}$10] direction. However, such modeling leads to 2D edge dislocations, which are clearly not seen in the image of Fig. 3a. Instead, this image shows nearly straight uninterrupted rows of Au atoms, implying that both types of ridge must include both compression along [001] and expansion along [$\bar{1}$10]. This feature also implies that the L2 structure is nearly that of a strain-relaxed Au net – i.e. a Au net transformed from pseudomorphic by uniform compression along [001] and uniform expansion along [$\bar{1}$10].

Fig. 4a shows that by overlaying such a Au net on a W(110) lattice one can accurately map the L2 structure observed in the STM and determine how it deviates from the strain-relaxed net. This mapping is generated by separating the second layer Au atoms into three groups: (1) those that lie within rectangular regions centered about the bcc binding sites (represented by open circles); (2) those that lie within rectangular regions centered about top sites (removed); (3) the remainder (filled circles). This illustrates for the actual structure that the atoms of the first group are nearly conformal to the previous layer through a shift into sites

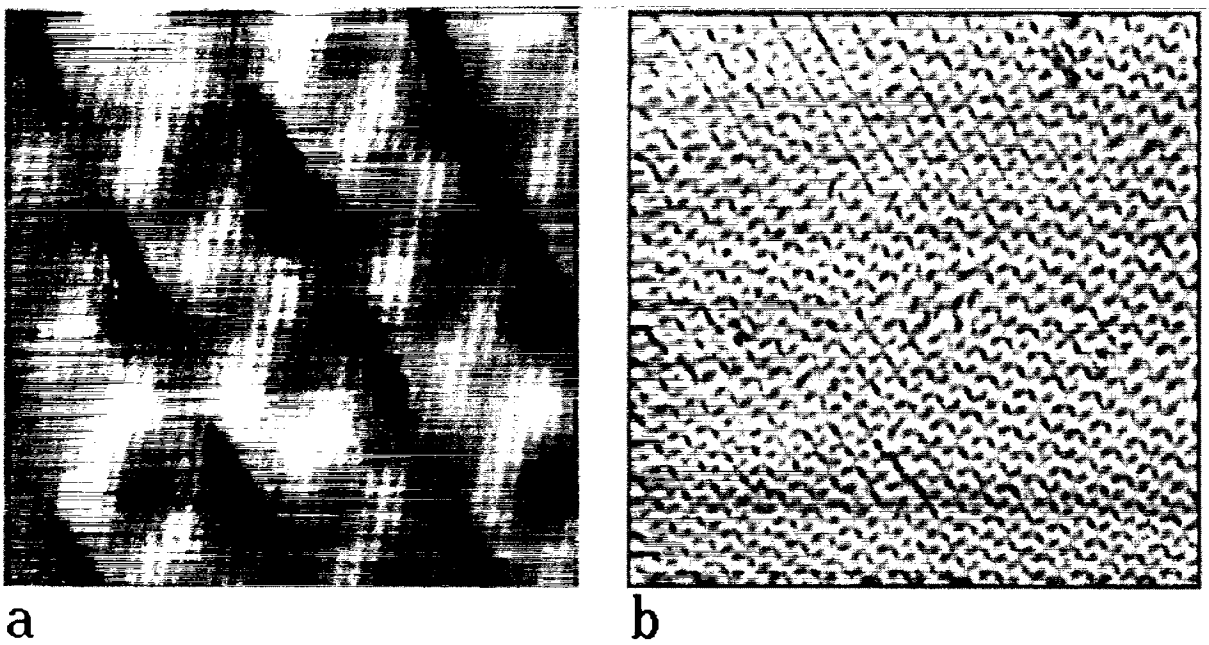

Fig. 3. STM images of layer 2. (a) Atomic-resolution image (100 Å × 100 Å) at 1.6 ML showing ridges with "square wave" pattern and periodically arranged vacancy rows. (b) (600 Å × 600 Å) image at 2.2 ML showing variability in orientational alignment.

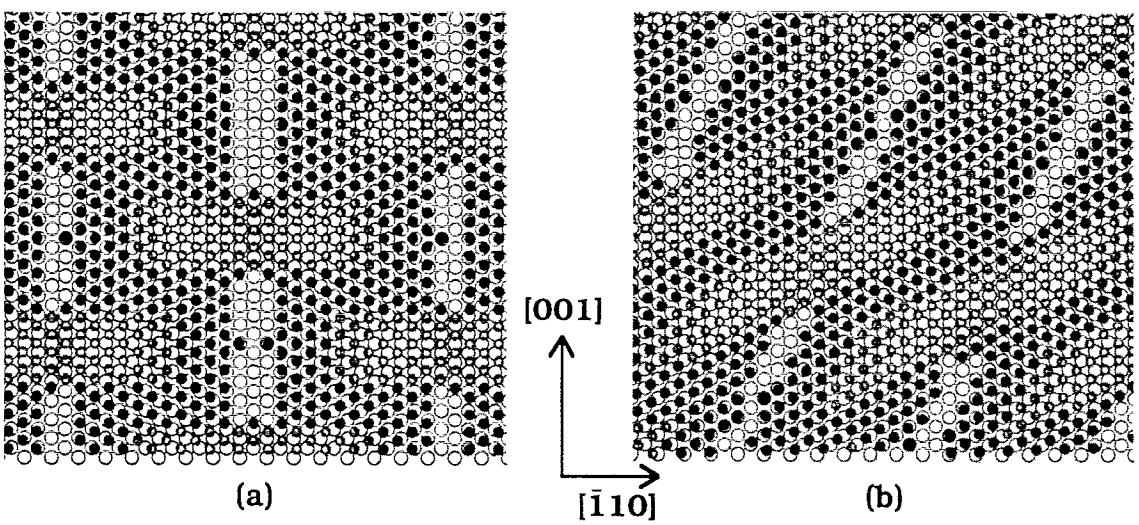

Fig. 4. Maps of the second-layer structure generated by overlaying a relaxed Au net on a W(110) lattice (dark open circles). In the actual Au structure the conformal regions are formed by the shifting into hollow sites of atoms located near the bcc sites (gray open circles) and the "square-wave" structure is formed by atoms predominantly in bridge sites (solid circles). The vacancy rows occur where the Au would be in top sites. (a) and (b) are maps for 0° and 2° orientations of the net respectively. The net, as determined from Fig. 3(a), is compressed by 4% along Au[$\bar{2}$11] and expanded by 1% along Au[01$\bar{1}$] compared with the fcc Au net.

that range approximately from the LH to the RH threefold sites, that the vacancy rows are due to a significantly smaller binding energy at top sites, and that the square-wave ridges are formed by atoms predominantly in bridge sites.

If bilayer films are formed by annealing deposits that slightly exceed 2 ML, Fig. 3b, then a more heterogeneous L2 structure is formed in which the Au net shows some variability in alignment. The square-wave structures are again evident in this image, but they change directions and some disorder can be seen in the regions separating different alignments. This orientational variability is not surprising given that this layer is nearly fully relaxed. Although the lateral atomic positions in a fully relaxed layer would be determined primarily by intra-layer atomic interactions, there would still be small strains induced by inter-layer atomic interactions that could be minimized by rotating the layer [11]. Apparently, intra-layer interactions are already predominant in L2, and such a rotation appears favored at the L1–L2 interface. However, inter-layer interactions are still appreciable since L2 is only near a fully relaxed structure and there is still a tendency for orientational alignment with the underlying layer.

By superimposing on Fig. 3a a net that is close to the imaged structure, it becomes clear that the second layer in this region is rotated with respect to the underlying lattice. By counting atomic spacings between the various features, the size of the mapping net and the rotation angle were determined and the map of Fig. 4b generated. The result is a net that is rotated by about 2° and that is much closer to the fcc geometry than the bcc one. Compared with the fcc Au net there is a 4% compression along the Au[$\bar{2}11$] direction and a 1% expansion along the Au[$01\bar{1}$] direction. This is in contrast to the pseudomorphic layer where both values are close to 10%.

Once again, as with the single-layer film, these STM observations require a reinterpretation of the LEED patterns. Previously, it was suggested that L2 was a hexagonal net compressed by 2.1–2.4% and rotated by 2.3–2.5° [9,10]. The STM does not reveal a uniform single atom net but a perturbation of one that results in a much larger multi-atom net. This perturbation should lead to additional diffraction beams, but only if it is sufficiently correlated over long length scales. The structural variability observed in STM confirms a lack of correlation and suggests that the LEED pattern results from a disordered multi-atom net that maintains enough long-range order to produce the strongest beams – the same ones produced by the single atom net. The quantitative differences between the present and previous models are small and are no doubt due to a highly localized measurement in STM on the one hand, and the large area average measurement in LEED on the other.

At 2.2 ML coverage, trilayer islands are found and they usually nucleate on the lower terrace at step edges. Fig. 5a shows a small trilayer island which extends across a step edge where the lower terrace shows an essentially unrotated "square wave" structure, much like Fig. 4a, whereas the upper bilayer terrace is primarily of the heterogeneous type. Running throughout the top of this trilayer island is a series of lines that are aligned along [$\bar{1}10$] and have a periodicity consistent with the L2 square-wave pattern. Superimposed on this line structure is an oblong domain structure that substantially breaks the mirror symmetry of the W(110) surface and can be seen in a second domain orientation on other island tops.

On top of larger trilayer islands, as illustrated in Fig. 5b, the film structure changes so that a substantially different pattern is imaged. This pattern is consistent with the Moiré or interference pattern constructed from an incommensurate isotropically relaxed overlayer on a W(110) lattice; this would not appear unless L2 changed to either a pseudomorphic layer or a relaxed layer identical to layer three (L3). The latter is most likely, since the exposed L2 showed considerable relaxation and the addition of L3 should induce further relaxation. Whether L1 has this same structure or remains pseudomorphic cannot be determined from the present data. The small trilayer islands, on the other hand, appear to be comprised of an isotropically relaxed third layer on top of the partially relaxed second layer "square wave" structure: the observed superimposed oblong domain and periodic line structures are consistent with the Moiré pattern constructed from this model.

When the coverage is increased above 3 ML the

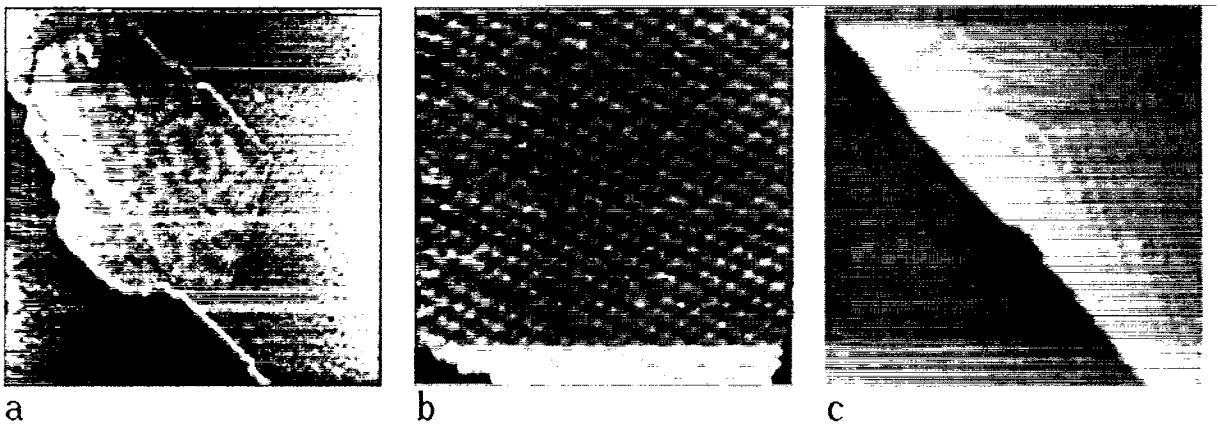

Fig. 5. (600 Å × 600 Å) STM images of layer 3. (a) Small L3 topped island at 2.2 ML that nucleated at step edge. The superposition of the oblong domain structure and the lines along [$\bar{1}$10] – which have a periodic arrangement matching the L2 structures on the terraces – is consistent with a fully relaxed third layer on top of an unchanged second layer. (b) Large L3 topped island at 2.2 ML where second layer has assumed a fully relaxed L3 structure. (c) Terraces covered by three layers at 3.6 ML. Upper right terrace has large island film structure in two possible orientations. Narrow terrace in lower left corner has small island film structure.

surface is nearly completely covered with the large island trilayer structure, but, in rare regions where the substrate steps are closely spaced, the small island trilayer structure can also be found. The lower left portion of Fig. 5c shows such a short terrace. In the upper right portion of this figure the film exhibits patterns that have two different orientations and that show some structural imperfections at the step edge due to structural transformations of underlying layers. Clearly, the relaxed layers of the trilayer film are rotated – and exhibit two energetically equivalent rotational domains – as a consequence of the strain energy dependence on the relative orientation of the Au and W lattices [11,12].

The existence of large and small island types of the trilayer film is apparently a size effect that may be described as follows. When considering only surface and interfacial energies, the third layer reduces the influence of the underlying substrate sufficiently to fully relax L2. However, the boundaries between such a trilayer film and a bilayer film have an energy cost, since they separate partially and fully relaxed regions of L2. This energy cost is sufficient to prevent full L2 relaxation at low L3 coverages. However, as more surface is covered with L3, the energy cost of maintaining the interface between the square-wave L2 and the relaxed L3 increases until it is greater than the energy cost of any structural discontinuities in L2 that would arise at the perimeter of the trilayer film.

3D growth is observed at coverages above 3 ML. The 3D islands that form nucleate at the step edges and are always an atomic step higher than the adjoining terrace so that the island tops correspond to at least layer five (L5). Fig. 6a shows a wide scan image at 3.6 ML which shows that many of these islands spill over adjacent steps while remaining flat topped so that a progression of film thicknesses may be observed in a single island. The junction of these islands to the step edge involves very sharp, oriented multiple height steps, as illustrated in Fig. 6b. Whereas this image shows some exposed layer four (L4), the combined observations of the commencement of 3D growth at 4 ML and the near overall absence of an exposed fourth layer suggests that there is a peak in the surface free energy as a function of film layer thickness: the surface free energy of the four-layer film is larger than that of either the three-layer or five-layer films.

Fig. 6c shows the transition from five-layer to six-layer film in the island of Fig. 6b. The diagonal

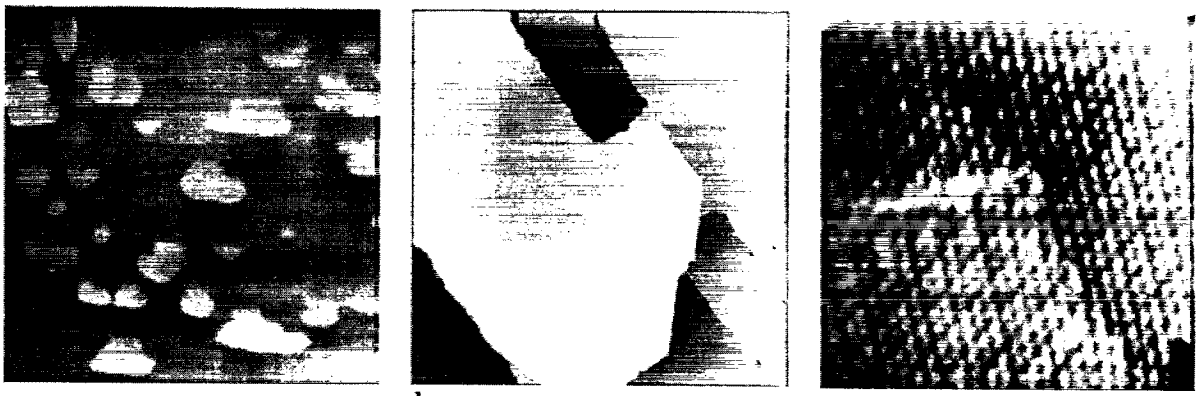

Fig. 6. STM images at 3.6 ML show onset of three dimensional growth. (a) (2 μm × 2 μm) image shows that islands nucleate at step edges and are flat topped. (b) (2000 Å × 2000 Å) image showing typical junction of island at step edge. The island has a top that is an atomic step higher than the adjoining terrace and it spills over onto a second lower terrace. The top is therefore comprised of L5 and L6. (c) (600 Å × 600 Å) image of L5–L6 transition of island seen in (b). The height discontinuity that extends from the lower right to the upper left is coincident with the underlying W step and is due to the difference in Au and W step heights. The linear defect originating at this layer transition is seen to extend to the island edge in image (b).

height discontinuity in this image corresponds to the difference between the step heights of the Au and W surfaces. An extended linear defect originates at this transition and continues to the island edge. It can also be seen that the lines of maximum height locations are not all continuous across the film transition. This shows that the six-layer film has a somewhat different structure than the five-layer film.

In rare cases, islands are found to extend over several steps, as in Fig. 7a. This image was recorded with high-pass filtering to reduce saturation effects of the six atoms high step at the upper island edge which corresponds to L9. Line defects are again seen to originate at the step crossings with the density and direction of these defects varying as the island thickens (Fig. 7a and b). Also, structural differences between successively thicker films are again evidenced by discontinuities in the lines of maximum height locations (Fig. 7c).

A possible explanation for these observations is that the trilayer film, though fully strain relaxed, is not bulk-like, and that as the film thickens it becomes more bulk-like. As the film does this, the surface layer experiences an increasing stress, as is known from the Au(111) reconstruction. So the surface layer begins to show dislocations. Initially these are few and far between, but they steadily increase in number. The dislocations show directional variability, since the changes in the underlying 2D periodicity parallel to the surface – resulting from the progression toward bulk structure – is likely to be anisotropic. By a film thickness of nine layers, the dislocations appear almost uniaxial and roughly aligned along the Au[$\bar{2}$11] direction, the direction of the Au(111) reconstruction lines.

When such a surface is subsequently coated with an additional 4 ML and annealed then these islands can further develop into very tall finger-like structures, as shown in Fig. 8a. Higher magnification images (not shown) of the base show the trilayer film structure. Fig. 8b is a higher magnification image of the top of one of the ten-atom-high fingers. At this thickness, steps do occur on these Au(111) structures, and it is still easy to detect the small height changes associated with substrate steps. There is also a paired stripe reconstruction on the island tops which matches the structure expected for a uniaxial $(22\times\sqrt{3})$ Au(111) surface. This reconstruction is seen with even higher magnification in Fig. 8c.

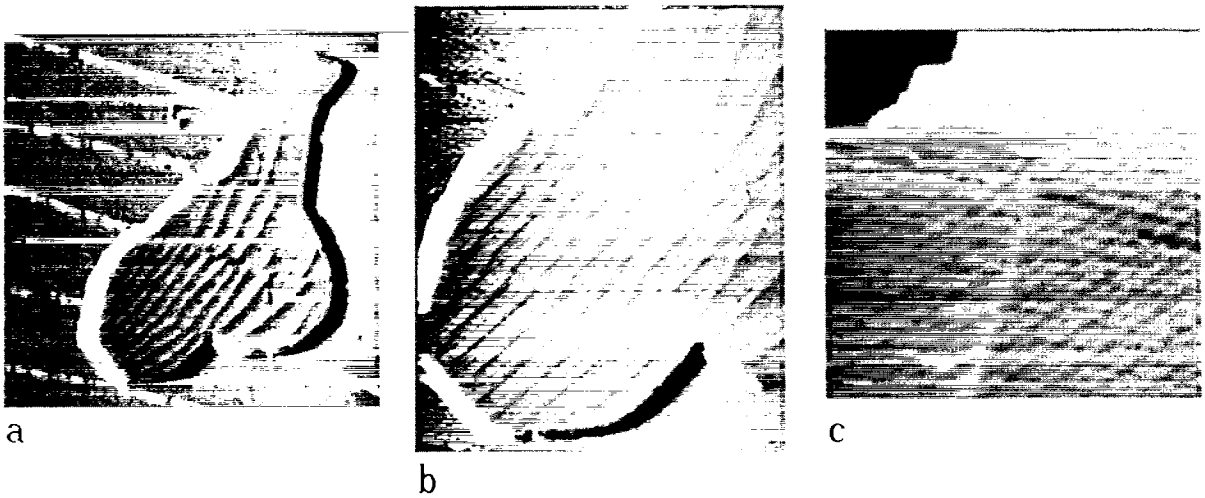

Fig. 7. STM images at 3.6 ML showing island that extends over five terraces so that flat top goes from L5 to L9. For L6 to L9, line defects span layer transition boundaries. Their orientation changes and their number density increases with increasing thickness. Their alignment at L9 is roughly along W[$\bar{1}$10] or Au[$\bar{2}$11], the direction of the Au(111) reconstruction lines. (a) Complete island (4000 Å × 4000 Å), (b) L7–L9 (1500 Å × 1750 Å), (c) L6–L7 (600 Å × 600 Å).

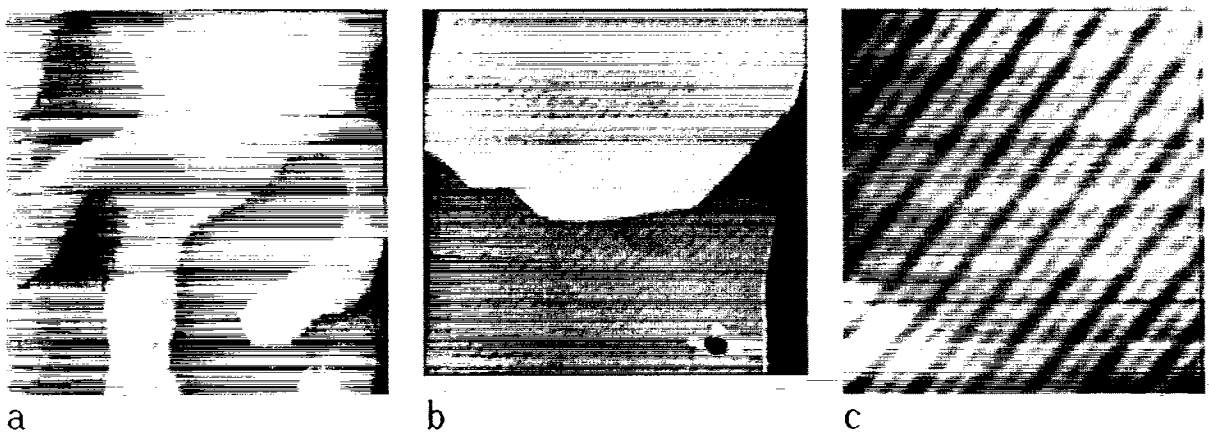

Fig. 8. STM images of surface that has been annealed to 500°C after 4 ML have been added to previously annealed 3.6 ML covered surface. (a) (2 μm × 2 μm) image shows very tall finger-like island on 3 ML covered terraces. (b) (2000 Å × 2000 Å) image on top of island. Au steps now appear on island top. There are two small height discontinuities associated with the W substrate steps running from middle right to upper left. The paired stripes of a Au(111) reconstruction are evident. (c) (450 Å × 450 Å) image on top of island gives high magnification view of reconstruction stripes.

In conclusion, this work shows a rich variety of surface, interfacial, and island growth structures in the formation of epitaxial films of Au on W(110). This richness is a consequence of the relaxation of both mixed strain in the heteroepitaxial system and tensile strain in the surface layer of Au. The atomic-resolution STM results are highly instructive: they both suggest atomic models that differ markedly from previously accepted models based on LEED and reveal unexpected island growth phenomena at elevated coverages. We expect that many subtle new phenomena will be

revealed by such high-resolution imaging techniques as other materials, film thicknesses, and deposition techniques are explored.

Acknowledgements

This work was supported in part by the Office of Naval Research (N00014-89-C-0099)

References

[1] R.J. Needs, M.J. Godfrey, M. Mansfield, Surf. Sci. 242 (1991) 215.
[2] F.C. Frank, J.H. van der Merwe, Proc. R. Soc. London Ser. A: 198 (1949) 205.
[3] C. Günther, J. Vrijmoeth, R.Q. Hwang, R.J. Behm, Phys. Rev. Lett. 74 (1995) 754.
[4] C. Wöll, S. Chiang, R.J. Wilson, P.H. Lippel, Phys. Rev. B 39 (1989) 7988.
[5] J.V. Barth, H. Brune, G. Ertl, R.J. Behm, Phys. Rev. B 42 (1990) 9307.
[6] H. Brune, H. Röder, C. Boragno, K. Kern, Phys. Rev. B 49 (1994) 2997.
[7] S. Chiang, R.J. Wilson, C. Gerber, V.M. Hallmark, J. Vac. Sci. Technol. A: 6 (1988) 386.
[8] R.Q. Hwang, J. Schröder, C. Günther, R.J. Behm, Phys. Rev. Lett. 67 (1991) 3279.
[9] E. Bauer, H. Poppa, G. Todd, P.R. Davis, J. Appl. Phys. 48 (1977) 3773.
[10] P.D. Augustus, J.P. Jones, Surf. Sci. 64 (1977) 713.
[11] J.P. McTague, A.D. Novaco, Phys. Rev. B 19 (1979) 5299.
[12] E. Bauer, J.H. van der Merwe, Phys. Rev. B 33 (1986) 3657.